Free Radical Biology and Medicine 221 (2024) 89–97

Contents lists available at ScienceDirect

Free Radical Biology and Medicine

journal homepage: www.elsevier.com/locate/freeradbiomed

Visualizing hydrogen peroxide and nitric oxide dynamics in endothelial cells using multispectral imaging under controlled oxygen conditions

Hamza Yusuf Altun [a,b,1], Melike Secilmis [a,b,1], Fan Yang [c], Tuba Akgul Caglar [a,b], Emre Vatandaslar [a], Muhammed Fatih Toy [d], Sven Vilain [a,**], Giovanni E. Mann [c,***], Gürkan Öztürk [a,e,****], Emrah Eroglu [a,b,*]

[a] Research Institute for Health Sciences and Technologies (SABITA), Istanbul Medipol University, 34810, Istanbul, Turkey
[b] Molecular Biology, Genetics, and Bioengineering Program, Sabanci University, 34956, Istanbul, Turkey
[c] King's British Heart Foundation Centre of Research Excellence, School of Cardiovascular and Metabolic Medicine & Sciences, Faculty of Life Sciences & Medicine, King's College London, 150 Stamford Street, London, SE1 9NH, UK
[d] School of Engineering and Natural Science, Istanbul Medipol University, 34810, Istanbul, Turkey
[e] Physiology Department, School of Medicine, Bolu Abant Izzet Baysal University (BAIBU), 14200, Bolu, Türkiye

ARTICLE INFO

Keywords:
Genetically encoded biosensors
Hydrogen peroxide
Nitric oxide
Multispectral imaging
Pericellular oxygen

ABSTRACT

The complex interplay between hydrogen peroxide (H_2O_2) and nitric oxide (NO) in endothelial cells presents challenges due to technical limitations in simultaneous measurement, hindering the elucidation of their direct relationship. Previous studies have yielded conflicting findings regarding the impact of H_2O_2 on NO production. To address this problem, we employed genetically encoded biosensors, HyPer7 for H_2O_2 and geNOps for NO, allowing simultaneous imaging in single endothelial cells. Optimization strategies were implemented to enhance biosensor performance, including camera binning, temperature regulation, and environmental adjustments to mimic physiological normoxia. Our results demonstrate that under ambient oxygen conditions, H_2O_2 exhibited no significant influence on NO production. Subsequent exploration under physiological normoxia (5 kPa O_2) revealed distinct oxidative stress levels characterized by reduced basal HyPer7 signals, enhanced H_2O_2 scavenging kinetics, and altered responses to pharmacological treatment. Investigation of the relationship between H_2O_2 and NO under varying oxygen conditions revealed a lack of NO response to H_2O_2 under hyperoxia (18 kPa O_2) but a modest NO response under physiological normoxia (5 kPa O_2). Importantly, the NO response was attenuated by L-NAME, suggesting activation of eNOS by endogenous H_2O_2 generation upon auranofin treatment. Our study highlights the intricate interplay between H_2O_2 and NO within the endothelial EA.hy926 cell line, emphasizing the necessity for additional research within physiological contexts due to differential response observed under physiological normoxia (5 kPa O_2). This further investigation is essential for a comprehensive understanding of the H_2O_2 and NO signaling considering the physiological effects of ambient O_2 levels involved.

1. Introduction

In cellular redox biology, the intricate interplay between nitric oxide (NO) and hydrogen peroxide (H_2O_2) has remained a long-standing challenge. The elusive nature of these reactive molecules, coupled with their transient existence within biological systems, has historically posed a challenge for researchers to understand their roles and regulatory mechanisms [1,2]. Recent advances have been catalyzed by the application of genetically encoded biosensors, which empower real-time visualization of reactive oxygen and nitrogen species (ROS/RNS) in

* Corresponding author. Research Institute for Health Sciences and Technologies (SABITA), Istanbul Medipol University, 34810, Istanbul, Turkey.
** Corresponding author.
*** Corresponding author.
**** Corresponding author. Research Institute for Health Sciences and Technologies (SABITA), Istanbul Medipol University, 34810, Istanbul, Turkey.
E-mail addresses: spvilain@medipol.edu.tr (S. Vilain), giovanni.mann@kcl.ac.uk (G.E. Mann), gozturk@medipol.edu.tr (G. Öztürk), emrah.eroglu@medipol.edu.tr (E. Eroglu).
[1] These authors contributed equally.

https://doi.org/10.1016/j.freeradbiomed.2024.05.021
Received 12 January 2024; Received in revised form 4 April 2024; Accepted 10 May 2024
Available online 11 May 2024

cellular models. These cutting-edge tools have brought us closer to understanding the dynamic behavior of NO and H_2O_2. However, unraveling the relationship between these two signaling molecules is not straightforward, as technical complexities inherent to *in vitro* systems continue to pose challenges in interpreting the nuanced interactions between these second messengers.

The introduction of HyPer biosensors in 2006 marked a significant turning point in the field of redox biology, revolutionizing our ability to unravel H_2O_2 dynamics [3] and significantly advancing our understanding of H_2O_2 dynamics within cellular systems. These biosensors have allowed us to define intricate processes governing the transport and subcellular localization of H_2O_2 [4,5]. Furthermore, the ability to visualize this reactive molecule has uncovered its characteristics as a second messenger and its modulation of redox signaling [6]. This has been instrumental in unraveling complex antioxidant response mechanisms and shedding light on the pivotal role of H_2O_2 in cancer [2]. The application of chemogenetic tools for manipulating the redox status of cells has enabled researchers to precisely modulate cellular redox states [7–11]. Thus, the utilization of HyPer biosensors has undeniably played a pivotal role in understanding cellular H_2O_2 dynamics.

A decade after the introduction of HyPer biosensors, we developed a biosensor for NO, geNOps, to monitor NO dynamics within subcellular locales [12]. The distinctive spectral properties of geNOps biosensors enabled multispectral imaging of subcellular NO levels [12–17]. We have obtained critical insights, including the diffusion of NO across biological membranes, the direct relationship between NO and calcium ions (Ca^{2+}), and the bioavailability of various NO donors and drugs metabolized to NO within cellular environments [14,15,18–20].

More recently, we provided novel insights into geNOps signaling under controlled pericellular oxygen (O_2) conditions encountered by cells *in vivo* [21]. We reported the first evidence that NO bioavailability was significantly increased in cells adapted to physiological normoxia (5 kPa O_2) compared to standard cell culture under atmospheric O_2 levels. Notably, our findings provided novel and critical insights: firstly, the susceptibility of fluorescent proteins to pericellular O_2 levels emerged, as FPs rely on O_2 for the maturation of their chromophore [21]. Under physiological normoxia, the significant increase in NO bioavailability was paralleled by substantial alterations in redox signaling and a dramatic disruption in ferrous iron uptake. Notably, the influence of oxygen extends beyond its modulation of ROS and RNS levels, as it exerts a key role in shaping the properties of the fluorescent proteins themselves, a factor that warrants careful experimental design [22]. Furthermore, we acknowledge that others have demonstrated the profound impact of pericellular O_2 culture conditions on key cellular parameters, including endothelial nitric oxide synthase (eNOS) levels and activity, antioxidant defense proteins, and Ca^{2+} signaling, all of which are intrinsically linked with and substantially influence the roles of H_2O_2 and NO within cellular systems [23–26]. These findings collectively emphasize the importance of the interplay between intracellular O_2 levels and the redox signaling landscape.

This study explores, for the first time, the direct relationship between H_2O_2 and NO in endothelial cells utilizing genetically encoded biosensors, within controlled atmospheric oxygen conditions with an emphasis on the optimum experimental settings.

2. Materials and methods

Molecular Cloning and Lentivirus production. Cytosolic targeted HyPer7 and O-geNOp constructs were subcloned into a 3rd generation lentivirus shuttle vector pLenti-MP2 (*Addgene #36097*), and HEK293T cells were used for lentivirus generation as described previously [27].

Cell Culture and Stable Cell Line Generation. The Human endothelial EA.hy926 cell line was purchased from ATCC (CRL-2922, Manassas, VA, USA). As previously described [21], EA.hy926 cells were maintained in Dulbecco's minimal essential medium (DMEM) (Pan Bio-tech, Aidenbach, Germany) supplemented with 10 % FBS (Pan Bio-tech, Aidenbach, Germany), 100 μg/mL Penicillin, 100 U/mL Streptomycin, 100 μg/mL Normocin (InvivoGen, San Diego, CA, USA), and 2 % HAT ((Sodium Hypoxanthine (5 mM), Aminopterin (20 μM), and Thymidine (0.8 mM)) (ATCC, Manassas, VA, USA) in a humidified CO_2 chamber (37 °C, 5 % CO_2). EA.hy926 cells were seeded in 6-well plates and upon achieving 50–60 % confluency, cells were transduced with respective lentivirus HyPer7 and O-geNOp, using an antibiotic-free transduction medium containing 10 % FBS and 10 μg/ml Polybrene for 48–72h. Cells expressing both Hyper7 and O-geNOp were selected using a fluorescence-activated cell sorter (FACS). The top 30 % of the cells expressing both HyPer7 and O-geNOp were sorted using a 488 nm laser (Filter: 530/40 nm) and 561 nm laser (Filter: 593/40 nm) on a BD Influx Cell Sorter. Sorted cells cultured using standard EA.hy926 culture protocols [20]. Before the day of an experiment, cells were seeded in a 6-well plates containing 30 mm coverslips (Glaswarenfabrik Karl Knecht Sondheim, Sondheim vor der Rhön, Germany).

Long-term adaptation of EA.hy926 cells in an oxygen controlled workstation. For oxygen controlled experiments, stably transfected EA.hy926 cells were maintained for at least 5 days in monolayer culture under 5 kPa (physiological normoxia) or 18 kPa (hyperoxia) O_2 in an oxygen-controlled Scitive dual workstation (Baker, USA). Adapting cells for 5 days ensures that physiological redox phenotype is achieved in the absence of HIF1-α stabilization [22,23]. Moreover, maintaining cells continuously within the workstation obviates the need for treatments of cells in a laminar flow hood under atmospheric oxygen [26].

Oxygen Controlled Plate Reader. EA.hy926 cells were plated in clear-bottom 96-well plates and pre-adapted for 5 days to either 18 kPa or 5 kPa O_2 in an oxygen-controlled Scitive dual workstation (Baker, USA). A time-resolved fluorescence plate reader (CLARIOStar, BMG Labtech) equipped with an atmospheric control unit was used for real-time imaging of Hyper7 or O-geNOp. Pre-adapted cells were rapidly transferred to the plate reader gassed with 18 or 5 kPa O_2 [25,28] to mimic oxygen levels in the workstation during pre-adaptation of cells. Excitation wavelengths were 420/20 nm (HyPer low) and 473/20 nm (HyPer high), and emissions were collected at 521/25 nm. Acute treatments of cells maintained under 18 or 5 kPa O_2 were applied using a dual injection system within the plate reader at the stated times and concentrations.

Iron Loading Procedure. Cells were pre-treated with Iron (II) supplementation (300 μM $FeSO_4$ and 500 μM ascorbate) for 15 min for full activation of the geNOps biosensor prior to experiments, as described previously [21].

Buffers and Solutions. All chemicals were purchased from Neo-Froxx unless otherwise stated. To maintain cells outside of the cell culture incubator, a cell storage buffer containing 2 mM $CaCl_2$, 5 mM KCl, 138 mM NaCl, 1 mM $MgCl_2$, 10 mM HEPES, 0.44 mM KH_2PO_4, 2.6 mM $NaHCO_3$, 0.34 mM NaH_2PO_4, 10 mM D-Glucose, 0.1 % MEM Vitamins (Pan-Biotech, Aidenbach, Germany), 0.2 % essential amino acids (Pan-Biotech, Aidenbach, Germany), 100 μg/mL Penicillin (Pan-Biotech, Aidenbach, Germany), and 100 U/mL Streptomycin (Pan-Biotech, Aidenbach, Germany) was used. The pH was adjusted to 7.42 using 1 M NaOH. The cell storage buffer was sterile filtered with a 0.45 μm medium filter (Isolab, Germany). For live-cell imaging experiments, a HEPES-buffered solution was used consisting of 2 mM $CaCl_2$, 5 mM KCl, 138 mM NaCl, 1 mM $MgCl_2$, 10 mM HEPES, 10 mM D-Glucose, and pH was adjusted to 7.42 using 1 M NaOH. Histamine (Sigma-Aldrich, MO, USA) was prepared as 100 mM stock solution and diluted to 100 μM for imaging experiments using HEPES-buffered solution. Auranofin (Sigma-Aldrich, MO, USA) was prepared as 7.36 mM in DMSO for a stock solution and diluted to 3 μM for imaging experiments using a HEPES-buffered solution. NOC-7 (Sigma Aldrich, MO, USA) was prepared as 50 μM stock solution and diluted to 1–10 μM for imaging experiments using HEPES-buffered solution. Final working concentrations of PEG-CAT and PEG-SOD (Sigma-Aldrich, UK) were prepared in DMSO 200 U/ml and 20 U/ml, respectively.

Widefield epifluorescence microscopy. Widefield epifluorescence

microscopy experiments were performed using a Zeiss Axio Observer Z1.7 (Carl Zeiss AG, Oberkochen, Germany), Plan-Apochromat 20 × /0.8 dry objective, Plan-Apochromat 40 × /1.4 oil immersion objective, a monochrome CCD camera Axiocam 503, and a custom-made gravity-based perfusion system. The optical path for HyPer7 starts with alternating excitation by 423/44 nm and 469/38 nm LED lights using a motorized filter wheel containing FT455 (HyPer low) and FT495 (HyPer high) beamsplitters (BS). Emissions were collected using the same emission filter (BP 525/50) in ratio imaging. For O-geNOp imaging, cells were excited with 555/30 nm LED light, and the filter combination is FT570 BS and 605/70 nm emission filter. The optical setup was the same, either mono-imaging or dual imaging of two biosensors. Data acquisition and control were set up using Zen Blue 3.1 Pro software (Carl Zeiss AG, Oberkochen, Germany). Provision and withdrawal of chemicals were conducted using an in-house gravity-based perfusion system connected to a perfusion chamber (NGFI, Graz, Austria).

Spinning Disk Microscopy. Spinning disk microscopy experiments were performed on a Zeiss Axio Observer.Z1 equipped with both Yokogawa CSU-X1 (Tokyo, Japan) confocal scanner unit and Colibri 2 as light sources. This microscope is also equipped with LD A-plan 20x/0.3 dry objective and 2 different cameras, QuantEM:512SC (Teledyne Photometrics, AZ, USA) and AxioHrm, for confocal mode measurements and widefield measurements, respectively. HyPer7 signals were obtained by exciting cells with a 488 nm laser, and emission was collected at 509 nm in confocal mode. In widefield mode, cells were excited using 470/20 nm LED light, and the filter set contains FT495 BS, 525/25 nm emission filter. O-geNOp measurements were performed by exciting cells with a 558 nm laser, and emission was collected at 589 nm in confocal mode. In widefield mode, cells were excited using 550/12 nm LED light, and the filter set contains FT570 BS, 605/35 nm emission filter. Chemicals were provided or withdrawn using a gravity-based perfusion system connected to the perfusion chamber.

Point Scanning Confocal Microscopy. Temperature experiments were performed on Zeiss AxioObserver equipped with LSM880 Confocal Laser Scan. To maintain and control ambient temperature microscope equipped with PeCon on-stage incubator (Erbach, Germany). For HyPer7 excitation, 405 nm and 488 nm lasers were used, and for O-geNOp excitation, a 543 nm laser was used with a multibeamsplitter (MBS). The microscope is also equipped with 32 channel GaAsp detector to collect emissions. Cells were imaged using Plan-Apochromat 20x/0.8 M27 objective.

Data Analysis. For O-geNOp signals, background subtraction was performed using Microsoft Excel. Basal fluorescence intensities were analyzed employing a one-phase decay function in GraphPad Prism software to normalize O-geNOp signals to 100 %. Raw fluorescence intensity is denoted as F, and normalized fluorescence intensity is denoted as F_0. To obtain normalized signal curves formula used below:

$$dF = (1-(F / F_0)) * 100$$

For HyPer7 signals, background subtraction was performed using Microsoft Excel. HyPer7 has two excitation and single emission termed HyPer low and HyPer high. The HyPer7 ratio was obtained by dividing HyPer high by HyPer low. Normalized HyPer ratios were obtained by normalizing HyPer ratios to their basal levels.

Statistical Analysis. All imaging data were analyzed using GraphPad Prism Software version 9 (GraphPad Software, San Diego, CA, USA). All experiments were performed at least three times and indicated as N/n where N represents the number of different experimental cultures and n represents the number of cells. All data denote mean ± S.E.M. unless stated otherwise. Statistical analysis of multiple groups was performed using one-way ANOVA with Tukey's posttest (Comparison of all pairs of columns). P-values are indicated as numerical values. For the comparison of multiple groups, the P-value was not indicated if the P-value was higher than 0.05. In order to compare two experimental conditions, an unpaired Student's *t*-test was performed. Statistical analysis of two groups was performed using unpaired Student's t-test or Welch's Student's t-test, as indicated in the figures.

3. Results

In order to simultaneously monitor intracellular levels of H_2O_2 and NO in endothelial cells, we established a transgenic cell line expressing the biosensors HyPer7 and O-geNOp through lentiviral transduction in EA.hy926 immortalized endothelial cells (Fig. 1A). Employing fluorescence-assisted cell sorting (FACS), we successfully enriched a cell population expressing both biosensors, achieving robust expression levels in 100 % of the cells (Fig. 1B). Subsequently, we rigorously assessed the functionality of these biosensors within the double-stable cell line by introducing controlled amounts of exogenous H_2O_2 or NO, enabling individual imaging of each biosensor (Fig. 1C and D).

We next conducted technical experiments to fine-tune multispectral imaging settings, enabling simultaneous measurement of these two different biosensors with high spatio-temporal resolution. First, we adjusted the camera binning settings to improve the signal-to-noise ratio (Supplementary Note 1). Increased pixel binning levels enhanced the HyPer7 response to H_2O_2 and altered the kinetics. Despite heightened background fluorescence, adjustments in excitation light intensity preserved unaffected background fluorescence. Notably, the 4 × 4 configuration resulted in the highest signal for accelerated H_2O_2 response (Figs. S1 and S2). In contrast, geNOp responses (both, O-geNOps and G-geNOps) to NOC-7 remained consistent across different binning settings, indicating minimal impact on geNOp's measurements (Figs. S1 and S4). However, when G-geNOp was measured with the same settings used for HyPer7, we observed a clear binning-dependent effect on the G-geNOps response (Fig. S4). Systematic testing revealed that both spinning disk (SD) and widefield (WF) microscopy are suitable for employing HyPer7 and O-geNOp biosensors. While SD microscopy provides higher contrast, maximum biosensor responses remained consistent between the two techniques, ensuring comparable performance for high-resolution live-cell imaging (Fig. S5 and Supplementary Note 2). Also, the impact of incubation temperature on biosensors, showed consistent behavior at both room temperature (RT) and physiological temperature (37 °C), with no significant effect on basal activity, response dynamics, or key parameters (Fig. S6 and Supplementary Note 3). Notably, these technical characterizations are crucial for accurately visualizing the precise relationship between H_2O_2 and NO signals in biological systems.

Building upon the outcomes of our prior optimization protocols, we proceeded to co-image both biosensors at room temperature (RT) under atmospheric (~18 kPa) O_2, employing a 4 × 4 camera binning setting on a conventional widefield microscope. Upon application of NOC-7, the O-geNOp signal reached a plateau, while the corresponding HyPer7 signal remained unaltered, signifying that exogenous NO does not acutely impact intracellular H_2O_2 levels (Fig. 2A and B). Subsequent exposure to extracellular H_2O_2 similarly failed to induce acute NO formation, as evidenced by O-geNOp signals (Fig. 2A and B). The alteration of the order of exogenous application, first H_2O_2 and then NOC-7, yielded comparable outcomes (Fig. S7), reinforcing that neither of these reactants triggers the immediate generation of the other molecule within the cell.

To assess endogenously generated NO and H_2O_2, we employed histamine, a G-protein-coupled receptor agonist, and Auranofin, a thioredoxin reductase inhibitor known to induce intracellular H_2O_2 accumulation [29]. Stimulation of NO production with histamine elicited an increase in O-geNOp signals but left HyPer7 signals unaffected (Fig. 2C and D). In contrast, Auranofin robustly elevated HyPer7 signals while leaving O-geNOp signals unaltered (Fig. 2C and D), indicating that under these optimized conditions, low levels of both reactive species can be accurately and dynamically detected.

We next investigated the impact of pericellular O_2 levels on cellular HyPer7 responses. Cells adapted to physiological normoxia (5 kPa O_2) for 5 days displayed distinct differences in NO signals, as detected by geNOps and reported in our previous study [21]. When incubated for 24

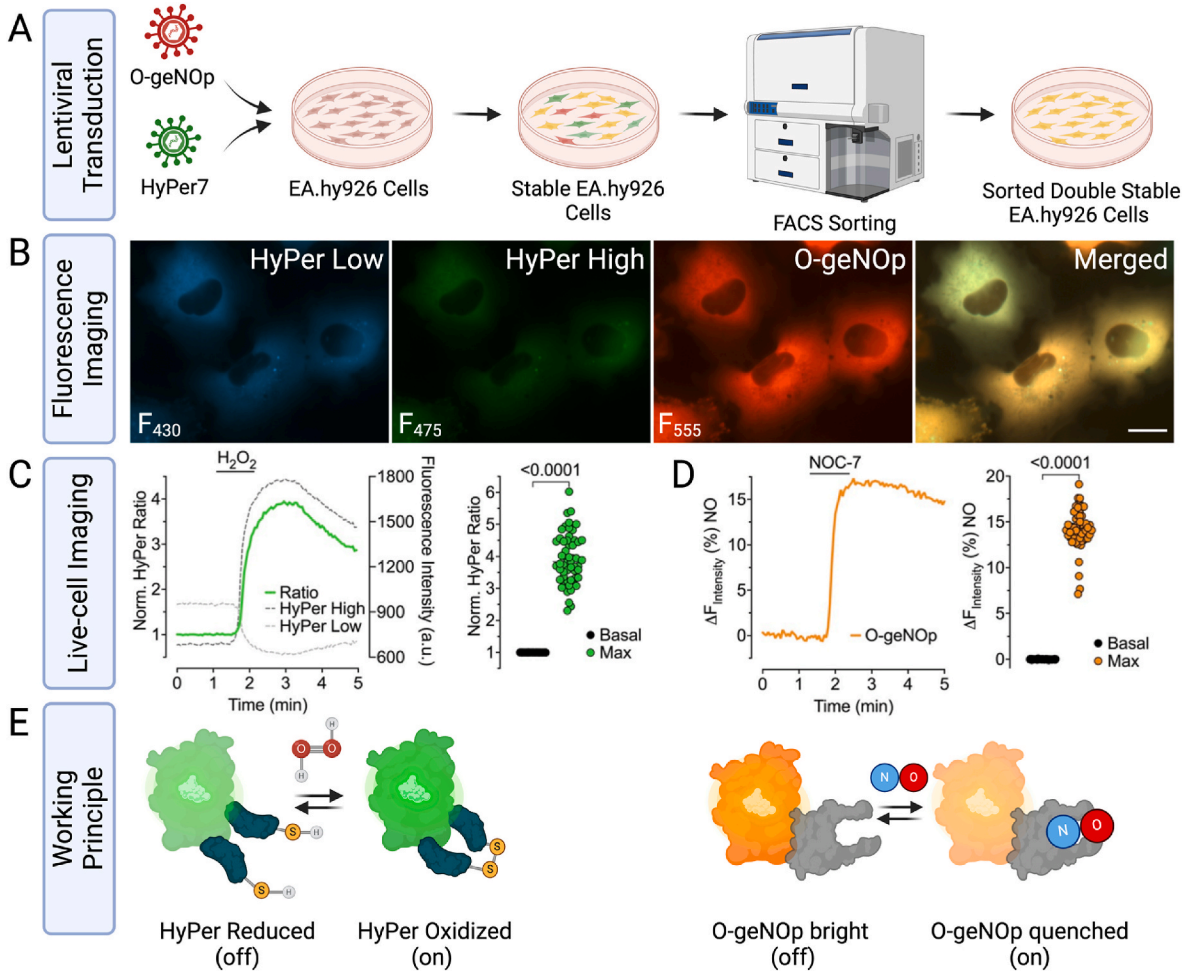

Fig. 1. Schematic overview and workflow for developing endothelial cells stably co-expressing HyPer7 and O-geNOp (A) Native endothelial cells (EA.hy926) at low passage were transduced with lentivirus containing ORFs of HyPer7 and O-geNOp, respectively. HyPer7 and O-geNOp expressing cells were sorted using FACS 48–72h after transduction. (B) Representative widefield images of endothelial cells after FACS. The first three panels show images of cells under different optical setups according to the optical properties of the biosensors HyPer low (Ex/Em: 430 nm/525 nm) (first image), HyPer high (Ex/Em: 475 nm/525 nm) (second image), O-geNOp (Ex/Em: 555 nm/605 nm) (third image) and fourth image shows merged channels. The scale bar represents 20 μm. (C) The representative green curve shows HyPer7 signals upon administration of 50 μM H_2O_2. The scatter dot plot shows basal levels (black dots, n = 3 cultures/57 cells) and maximum HyPer7 responses (green dots, n = 3/57) of individual cells. (D) Representative orange curve shows O-geNOp signals after the provision of 10 μM NOC-7. The scatter dot plot shows O-geNOp responses under basal levels (black dots, n = 3/57) and maximum responses upon administration of 10 μM NOC-7 (orange dots, n = 3/57), $P < 0.0001$, Student's t-test. (E) Schematics illustrate the working principle of HyPer7 and O-geNOp biosensors, respectively.

h and challenged with Auranofin, we observed a significant and robust HyPer7 signal (Fig. 3A–B). Intriguingly, cells adapted to physiological normoxia for 5 days (Supplementary Note 4) exhibited a diminished H_2O_2 response to the same agonist, initially raising concerns about biosensor functionality (Fig. 3A–B). However, control experiments applying low levels of exogenous H_2O_2 revealed that the biosensor functioned equally well under both O_2 conditions (Fig. 3C–D). Notably, cells adapted to atmospheric O_2 (18 kPa) maintained stable HyPer7 signals over time, while in cells adapted to 5 kPa O_2 signals rapidly returned to baseline (Fig. 3C–D). These findings suggest that cells maintained under atmospheric O_2 conditions have higher basal oxidative stress levels and a potentially lower antioxidant capacity compared to cells under physiological normoxia (5 kPa O_2).

To support these findings, we further examined the potential influence of varying O_2 levels on basal intracellular antioxidant enzymes. EA.hy296 cells were adapted to physiological normoxia (5 kPa O_2) and then challenged with Auranofin alone or in the presence of PEG-Catalase or PEG-SOD to scavenge H_2O_2 or superoxide anions, respectively (Fig. 4A). Notably, there were no discernible differences between control and PEG-SOD-treated cells. However, PEG-Catalase treated cells exhibited reduced HyPer7 signals, indicating an accumulation of H_2O_2 in response to Auranofin, rather than $O_2^{\cdot-}$. We repeated this experimental setup with cells adapted to 18 kPa O_2 (Fig. 4B) and noted that H_2O_2 generation in response to Auranofin was significantly faster with a higher amplitude (Fig. 4C–D). These findings establish a critical role of pericellular O_2 levels in modulating cellular redox responses, as highlighted by the use of genetically encoded biosensors. These observations provide critical insights into the dynamic interplay between oxidative stress and cellular antioxidant defenses under defined O_2 conditions and may have wide-reaching implications for other cell types [30].

We next investigated the relationship between H_2O_2 and NO under varying O_2 levels. Endothelial cells expressing both HyPer7 and O-geNOp were maintained under 18 kPa or 5 kPa O_2 for at least 5 days. During the imaging experiments, cells were briefly exposed to H_2O_2 under 5 and 18 kPa O_2 conditions (Fig. 5A–B). Notably, basal HyPer7 ratios were lower in 5 kPa consistent with previous experiments (Figs. 3C and 5C, left panel). Similar to the results shown above (Fig. 3D), the administration of 25 μM H_2O_2 elicited robust HyPer7 responses (Fig. 5C, middle panel). Notably, under these conditions, H_2O_2 treatment in endothelial cells did not yield an O-geNOp response,

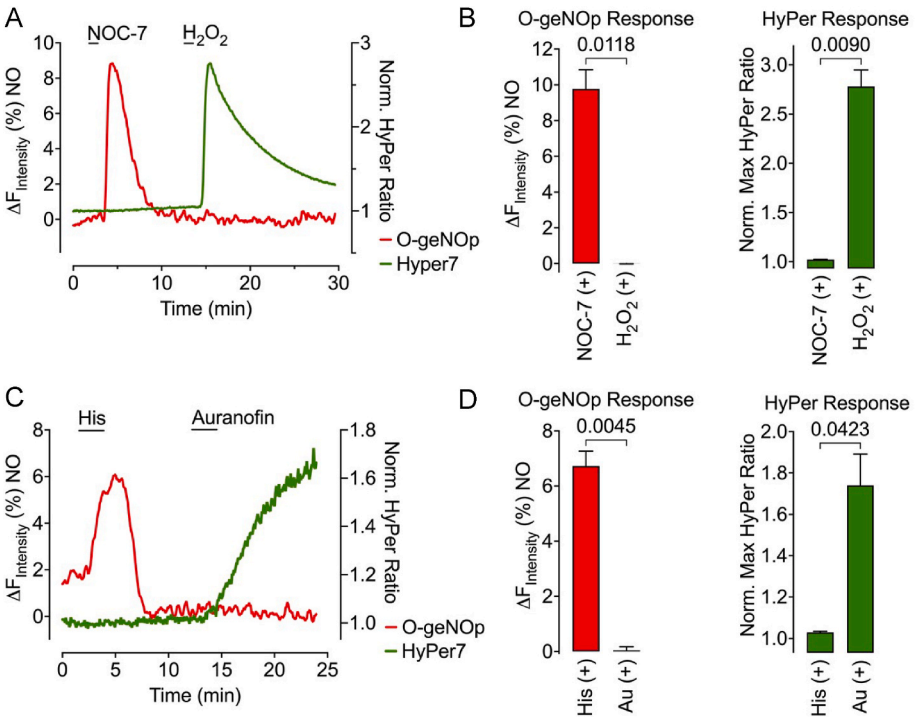

Fig. 2. Simultaneous imaging of exogenously and endogenously induced H_2O_2 and NO. (A) Average curves represent simultaneous measurements of exogenously induced NO and H_2O_2 detected by O-geNOp (red curve) and HyPer7 (green curve) biosensors, respectively. Cells expressing both O-geNOp and HyPer7 biosensors were stimulated with 1 μM NOC-7 and 25 μM H_2O_2, respectively (n = 3/30). (B) The bar plot indicates the maximum responses of O-geNOp signal (red bar, left) and the maximum responses of HyPer7 signal (green bar, right) when cells were stimulated by 1 μM NOC-7 and 25 μM H_2O_2. (C) Average curves represent simultaneous measurements of endogenously induced NO and H_2O_2 detected by O-geNOp (red curve) and HyPer7 (green curve) biosensors, respectively. Cells expressing both O-geNOp and HyPer7 biosensors were stimulated with 30 μM histamine or 3 μM Auranofin, respectively (n = 3/38). (D) The bar plot indicates the maximum responses of O-geNOp signal (red bar, left) and the maximum responses of HyPer7 signal (green bar, right) in response to 30 μM histamine and 3 μM Auranofin. Data denote mean ± S.E.M. Statistical significance was obtained using Student's t-test, and P-values are indicated in bar plots.

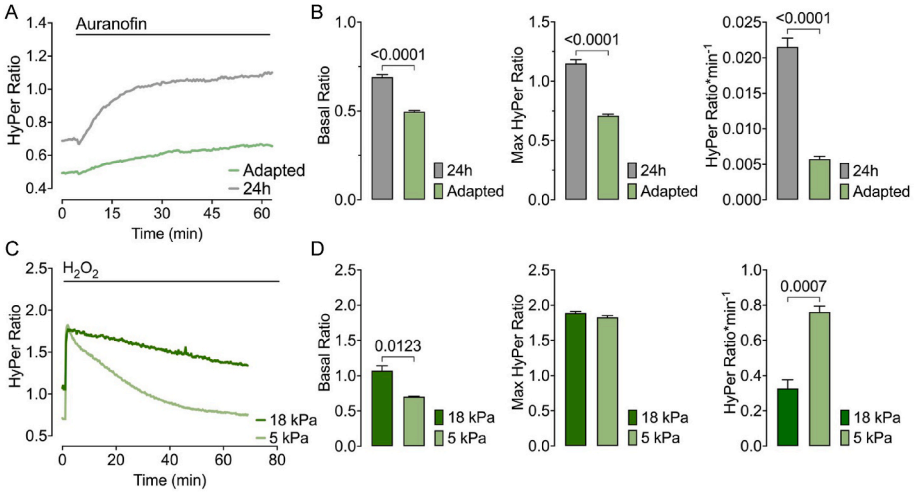

Fig. 3. Long-term adaptation to physiological normoxia affects intracellular H_2O_2 levels. (A) HyPer7.expressing EA.hy926 cells were adapted to 5 kPa O_2 for 5 days (adapted, light green line) or 24 h (24h, grey line). Cells were injected with 1 μM Auranofin using a microinjector in a CLARIOstar plate reader and HyPer7 ratios monitored (n = 3/25). (B) The left panel shows basal HyPer7 ratios. The middle panel shows maximum ratio amplitudes in cells in response to 1 μM auranofin. The right panel shows the H_2O_2 generation rate when cells were challenged with 1 μM auranofin. (C) Representative curves show HyPer7 expressing EA.hy926 cells that were adapted to either 18 kPa O_2 (dark green) or 5 kPa O_2 (light green) for 5 days. Cells were acutely treated with 10 μM H_2O_2 using a microinjector in a CLARIOstar plate reader and HyPer7 responses were measured under 18 or 5 kPa O_2 environment (n = 3/10). (D) The left panel shows basal HyPer7 ratios. The middle panel indicates maximum responses of cells to 10 μM exogenous H_2O_2. The right panel represents H_2O_2 scavenging rate expressed as a decrease in the HyPer7 ratio over time. Data denote mean ± S.E.M. Statistical significance using Student's t-test, and P-values are indicated in bar plots.

indicating that the treatment of endothelial cells with exogenous H_2O_2 has marginal effects on NO production (Fig. 5C, right panel).

We then explored whether endogenous H_2O_2 formation affects NO levels in cells adapted to different O_2 levels. Following 5 days of adaptation under 18 kPa or 5 kPa O_2, cells were acutely exposed to auranofin while simultaneously recording HyPer and geNOps signals (Fig. 5D–E).

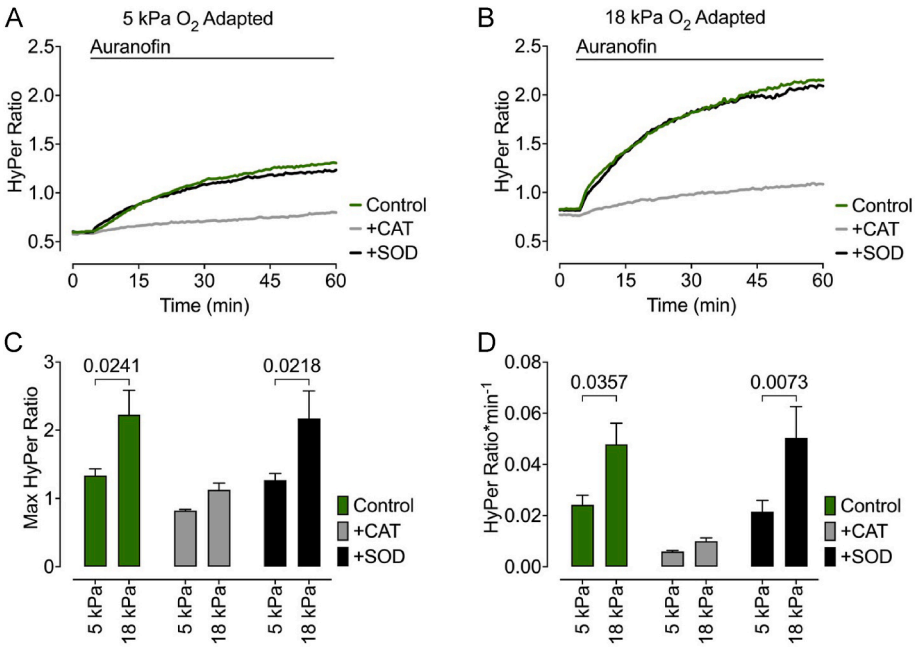

Fig. 4. Catalase but not SOD attenuates Auranofin-mediated HyPer7 signals under atmospheric O_2 (18 kPa) and physiological O_2 (5 kPa). (A) EA.hy926 cells expressing HyPer7 were adapted for 5 days to 5 kPa O_2 levels and 2 h prior to an experiment were treated with 200 U/ml PEG-CAT (grey line) or 20 U/ml PEG-SOD (black line). Cells were challenged with 1 μM Auranofin using the microinjector system in the oxygen controlled plate reader. (B) The same experimental setup and treatments were used as in panel A, but cells were adapted to 18 kPa O_2. (C) Bars represent the statistical analysis of the maximum HyPer7 ratio in response to acute 1 μM Auranofin in cells adapted to either 5 or 18 kPa O_2 and treated with PEG-CAT (grey bars) or PEG-SOD (black bars). The green bars represent control cells in the absence of either PEG-CAT or PEG-SOD. (D) Bars indicate the rate of HyPer7 ratio change in response to acute 1 μM Auranofin in cells adapted to either 5 or 18 kPa O_2 and treated with PEG-CAT (grey bars) or PEG-SOD (black bars). The green bars represent control cells in the absence of either PEG-CAT or PEG-SOD. Repeats for all experiments: n = 3/14. Data denote mean +S.E.M. and 2-way ANOVA multiple comparison test used to determine significance.

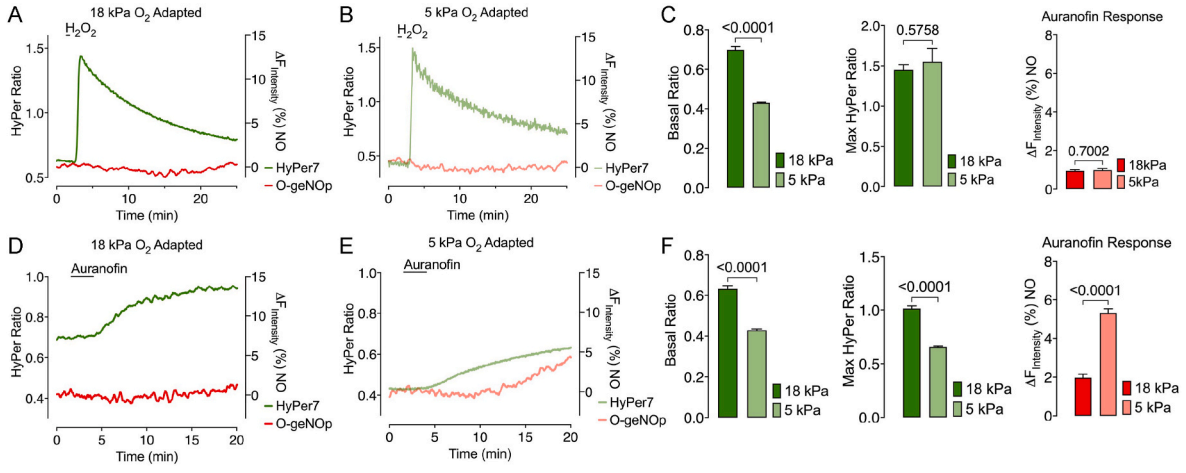

Fig. 5. Simultaneous imaging of exogenously and endogenously induced H_2O_2 and NO in cells adapted to either atmospheric O_2 (18 kPa) or physiological O_2 (5 kPa). (A) EA.hy926 cells expressing both HyPer7 and O-geNOp adapted 18 kPa O_2 level were perfused with 25 μM H_2O_2, and HyPer7 (dark green) and O-geNOp (dark red) signals were traced using fluorescence microscopy (n = 3/45). (B) The same experimental setup was used as in panel A, but cells were adapted to 5 kPa O_2 for 5 days, and HyPer7 (light green) and O-geNOp (light red) signals were monitored (n = 3/43). (C) The left panel shows basal HyPer7 ratios in cells adapted to 5 kPa (light green) and 18 kPa (dark green). The middle panel shows maximum HyPer7 ratio amplitudes in cells in response to 25 μM H_2O_2. The right panel indicates NO production upon 25 μM H_2O_2 stimulation in cells adapted to 5 kPa (light red) and 18 kPa (dark red). (D) EA.hy926 cells expressing both HyPer7 and O-geNOp adapted 18 kPa O_2 level were perfused with 3 μM Auranofin, and HyPer7 (dark green) and O-geNOp (dark red) signals were traced using fluorescence microscopy (n = 3/45). (E) The same experimental setup was used as in panel D, but cells were adapted to 5 kPa O_2 for 5 days, and HyPer7 (light green) and O-geNOp (light red) signals were traced (n = 3/40). (F) The left panel shows basal HyPer7 ratios in cells adapted to 5 kPa (light green) and 18 kPa (dark green). The middle panel shows maximum HyPer7 ratio amplitudes in cells in response to 3 μM Auranofin. The right panel shows NO production upon 3 μM Auranofin stimulation in cells adapted to 5 kPa (light red) and 18 kPa (dark red). Data denote mean ± S.E.M. Statistical significance was obtained using Student's *t*-test, and P-values are indicated in bar plots.

Auranofin treatment induced a strong HyPer7 signal under both O_2 conditions, yet the response was marginally delayed under 5 kPa O_2, (Fig. 5E). Additionally, basal HyPer7 ratios were lower under 5 kPa O_2 (Fig. 5F, left panel). The magnitude of auranofin-induced H_2O_2 production differed significantly, as observed previously (Fig. 5F, middle panel). Intriguingly, after the auranofin challenge, NO signals gradually increased in cells cultured under 5 kPa O_2 but not in cells cultured under 18 kPa O_2 (Fig. 5F, right panel). To validate the origin of

NO signals, experiments were conducted using L-NAME, an inhibitor for eNOS that prevents NO production. The diminished NO response implies that NO levels may be derived from eNOS (Fig. S8).

Since eNOS activity relies on calcium, it is surprising that auranofin treatment did not trigger any Ca^{2+} changes in endothelial cells under these experimental conditions (Fig. S9).

4. Discussion

In this study, we employed multispectral imaging techniques to simultaneously measure HyPer7 and O-geNOp signals in endothelial cells stably expressing both biosensors, aiming to investigate the impact of H_2O_2 on NO levels. Our approach involved (i) establishing double stable EA.hy926 cells expressing the biosensors, (ii) optimizing microscopic and environmental parameters to optimize multispectral signal acquisition, (iii) exploring the influence of pericellular O_2 levels (physiological normoxia vs. hyperoxia) on biosensor functionality and understanding cellular responses to exogenous and endogenous H_2O_2 challenges. Our optimization of experimental protocols enabled us to further elucidate the relationship between H_2O_2 and NO in endothelial cells.

The spectral distance between fluorescent biosensors HyPer7 and O-geNOp allows independent measurements of both analytes. Hence, multispectral imaging is an excellent method for studying the direct interaction between H_2O_2 and NO in single endothelial cells. However, transient transfection methods are inefficient in the endothelial cell line EA.hy926 [31,32]. Hence, a transgenic methodology via viral transduction was used to generate cell lines expressing both HyPer7 and O-geNOp simultaneously (Fig. 1). Functionality tests have shown that the probes are fully functional. Even though lentiviral vectors readily integrate into the host genome, their integration sites tend to be random [33]. Random integration of the open reading frame of a genetically encoded biosensor bears the risk of non-functional genetically encoded biosensors and may destroy endogenous gene expression patterns essential for cell function [34,35]. To limit these risks, instead of generating single double-stable clones of EA.hy926 cells, we used polyclones to obtain a mixed cell population. One of the significant benefits of stable cell lines is that biosensor integration remains stable over long passages. Thus, future studies might employ gene editing approaches to selectively integrate the biosensors to so-called safe-harbor locations [36] to ensure that the physiological state of cells is not altered.

We employed optimized parameters to simultaneously measure the effects of exogenous and endogenous generated H_2O_2 and NO in human endothelial cells. We selected a conventional widefield microscope and successfully monitored exogenous and endogenous induced changes in H_2O_2 and NO biosensor signals (Fig. 2), with negligible influence of H_2O_2 on NO. In a recent study, we demonstrated that pericellular O_2 levels have a significant impact on NO bioavailability in endothelial cells under physiological normoxia [21,23].

To our knowledge, the HyPer7 biosensor has not been tested systematically under different O_2 conditions. To address this knowledge gap, we compared the functionality of HyPer7 under atmospheric (18 kPa) and normoxic (5 kPa) O_2 levels. Intriguingly, we observed significant disparities in HyPer7 signals in cells adapted to 5 kPa O_2 for durations of 24 h and 5 days. We have previously established that cells require adaptation to normoxic O_2 levels encountered *in vivo* for at least 5 days to obtain a physiological redox phenotype in the absence of HIF-1α stabilization [22,26]. In Fig. 3, we established for the first time that basal HyPer7 ratio levels were increased in cells adapted to hyperoxic O_2 levels, indicating an elevated baseline of reactive oxygen species generation. Furthermore, the decay in the HyPer7 signal in hyperoxia-adapted cells was delayed, whereas the signal in cells adapted to physiological normoxia (5 kPa O_2) rapidly returned to baseline. These observations raise important concerns about disrupted antioxidant levels in cells cultured under standard atmospheric O_2 conditions [26]. These data suggest that intracellular antioxidant defenses may be dysregulated or overwhelmed by the redox distress experienced by cells adapted to hyperoxia (Fig. 4) [23,30]. Previous research has indicated an attenuated induction of antioxidant defense enzymes regulated by NFR2 in cells adapted to physiological normoxia in mouse brain microvascular and human coronary artery and umbilical vein endothelial cells [25,26,37].

When we examined the relationship between H_2O_2 and NO under physiological normoxia and hyperoxia, we noted that a brief exposure to H_2O_2 did not trigger NO production in either O_2 environment. However, upon endogenous H_2O_2 generation via auranofin, a substantial increase in NO levels was observed under physiological normoxia, a response that was validated using the eNOS inhibitor L-NAME. Although eNOS is a cytoplasmic Ca^{2+}-dependent enzyme, surprisingly, Ca^{2+} imaging using Fura-2 AM in response to auranofin did not reveal any calcium fluctuations. Similar findings were reported in HUVEC, where treatment with oleanolic acid elevated NO without affecting Ca^{2+} levels [38]. Calcium-independent eNOS activation via eNOS phosphorylation at Serine 1177 is well-established yet controversially discussed [20]. A recent study investigating the relationship between H_2O_2 and eNOS using chemogenetic tools showed a clear time concentration-dependent relationship between H_2O_2 and eNOS phosphorylation [9]. Moreover, this study demonstrates that intracellularly generated H_2O_2 had a greater phosphorylation effect on $eNOS^{S1177}$ compared to exogenously applied H_2O_2 [9]. Additionally, previous studies in HUVEC suggested that the rate of $eNOS^{S1177}$ phosphorylation under physiological normoxia declines over time following histamine stimulation [22]. Historically, scientists have regarded $eNOS^{S1177}$ phosphorylation as an indicator of eNOS activity. However, a more recent study challenges this phenomenon, suggesting that $eNOS^{S1177}$ phosphorylation per se does not affect eNOS activation and NO production in endothelial cells [20].

5. Conclusions

To our knowledge, our study is the first to investigate the relationship between H_2O_2 and NO signals under varying oxygen levels in endothelial cells. Under standard, hyperoxic cell culture conditions, we found no evidence supporting the notion that either intracellular or extracellular H_2O_2 significantly affects intracellular NO generation. Importantly, basal and auranofin-stimulated intracellular H_2O_2 levels were significantly lower in endothelial cells adapted to physiological O_2 levels compared to cells cultured under atmospheric oxygen, which is well-known to upregulate NRF2-targeted cellular antioxidant defenses [22,25,26,37]. Under physiological, normoxic oxygen levels, we observed only little increases in NO signals upon auranofin-mediated H_2O_2 increase in the absence of intracellular calcium activation.

CRediT authorship contribution statement

Hamza Yusuf Altun: Visualization, Validation, Methodology, Investigation, Formal analysis, Data curation. **Melike Secilmis:** Visualization, Validation, Methodology, Investigation, Formal analysis, Data curation. **Fan Yang:** Visualization, Validation, Methodology, Investigation, Formal analysis, Data curation. **Tuba Akgul Caglar:** Visualization, Validation, Methodology, Investigation, Formal analysis, Data curation. **Emre Vatandaslar:** Visualization, Methodology. **Muhammed Fatih Toy:** Writing – review & editing, Formal analysis. **Sven Vilain:** Writing – review & editing, Writing – original draft, Conceptualization. **Giovanni E. Mann:** Writing – review & editing, Writing – original draft, Supervision, Resources, Conceptualization. **Gürkan Öztürk:** Writing – review & editing, Writing – original draft, Supervision, Resources, Conceptualization. **Emrah Eroglu:** Writing – review & editing, Writing – original draft, Visualization, Validation, Supervision, Project administration, Methodology, Investigation, Funding acquisition, Data curation, Conceptualization.

Declaration of competing interest

The authors declare the following financial interests/personal relationships which may be considered as potential competing interests: Emrah Eroglu reports financial support was provided by European Molecular Biology Organization. Hamza Yusuf Altun reports financial support and travel were provided by European Molecular Biology Organization. Hamza Yusuf Altun reports financial support and travel were provided by European Cooperation in Science and Technology. Emrah Eroglu reports financial support was provided by Scientific and Technological Research Council of Turkey. Hamza Yusuf Altun reports financial support was provided by Scientific and Technological Research Council of Turkey. Melike Secilmis reports financial support was provided by Scientific and Technological Research Council of Turkey. Tuba Akgul Caglar reports financial support was provided by Scientific and Technological Research Council of Turkey. The authors declare that they have no known competing financial intersts or personal relationships that could have appeared to influence the work reported in this paper. If there are other authors, they declare that they have no known competing financial interests or personal relationships that could have appeared to influence the work reported in this paper.

Acknowledgments

We gratefully acknowledge support from the Scientific and Technological Research Council of Turkey Grant 2232 (118C242, M.S., H.Y.A., T.A.C., E.E.), EMBO Scientific Exchange Grants (H.Y.A.), EMBO IG (4113, E.E.) and European Cooperation in Science and Technology COST Action CA20121 '**Ben**ch to **Bed**side transition for **Phar**macological regulation of NRF2 in non-communicable diseases' (G.E.M., H.Y.A., E.E.). We thank Dr. R.C.M. Siow for research support at King's College London (Stavanger University Hospital). Fig. 1 was created with BioRender.com (Agreement number: MI24VDYK0T). HyPer7 plasmids were generously provided by Vsevolod Belousov.

Appendix A. Supplementary data

Supplementary data to this article can be found online at https://doi.org/10.1016/j.freeradbiomed.2024.05.021.

References

[1] D.D. Thomas, X. Liu, S.P. Kantrow, J.R. Lancaster, The biological lifetime of nitric oxide: implications for the perivascular dynamics of NO and O2, Proc. Natl. Acad. Sci. U. S. A. 98 (2001) 355–360.

[2] C. Lennicke, J. Rahn, R. Lichtenfels, L.A. Wessjohann, B. Seliger, Hydrogen peroxide – production, fate and role in redox signaling of tumor cells, Cell Commun. Signal. 13 (2015) 39, https://doi.org/10.1186/s12964-015-0118-6.

[3] V.V. Belousov, A.F. Fradkov, K.A. Lukyanov, D.B. Staroverov, K.S. Shakhbazov, A. V. Terskikh, S. Lukyanov, Genetically encoded fluorescent indicator for intracellular hydrogen peroxide, Nat. Methods 3 (2006) 281–286, https://doi.org/10.1038/nmeth866.

[4] V.V. Pak, D. Ezeriņa, O.G. Lyublinskaya, B. Pedre, P.A. Tyurin-Kuzmin, N. M. Mishina, M. Thauvin, D. Young, K. Wahni, S.A. Martínez Gache, A. D. Demidovich, Y.G. Ermakova, Y.D. Maslova, A.G. Shokhina, E. Eroglu, D.S. Bilan, I. Bogeski, T. Michel, S. Vriz, J. Messens, V.V. Belousov, Ultrasensitive genetically encoded indicator for hydrogen peroxide identifies roles for the oxidant in cell migration and mitochondrial function, Cell Metabol. 31 (2020) 642–653.e6, https://doi.org/10.1016/j.cmet.2020.02.003.

[5] C. Krüger, M. Waldeck-Weiermair, J. Kaynert, T. Pokrant, Y. Komaragiri, O. Otto, T. Michel, M. Elsner, AQP8 is a crucial H2O2 transporter in insulin-producing RINm5F cells, Redox Biol. 43 (2021) 101962, https://doi.org/10.1016/j.redox.2021.101962.

[6] C.M. Brown, Fluorescence microscopy - avoiding the pitfalls, J. Cell Sci. 120 (2007) 1703–1705, https://doi.org/10.1242/jcs.03433.

[7] Y.C. Erdogan, H.Y. Altun, M. Secilmis, B.N. Ata, G. Sevimli, Z. Cokluk, A.G. Zaki, S. Sezen, T. Akgul Caglar, İ. Sevgen, B. Steinhorn, H. Ai, G. Öztürk, V.V. Belousov, T. Michel, E. Eroglu, Complexities of the chemogenetic toolkit: differential mDAAO activation by d-amino substrates and subcellular targeting, Free Radic. Biol. Med. 177 (2021) 132–142, https://doi.org/10.1016/j.freeradbiomed.2021.10.023.

[8] B. Steinhorn, E. Eroglu, T. Michel, Chemogenetic approaches to probe redox pathways: implications for cardiovascular pharmacology and toxicology, Annu. Rev. Pharmacol. Toxicol. 62 (2022) 551–571, https://doi.org/10.1146/annurev-pharmtox-012221-082339.

[9] S.S. Saeedi Saravi, E. Eroglu, M. Waldeck-Weiermair, A. Sorrentino, B. Steinhorn, V. Belousov, T. Michel, Differential endothelial signaling responses elicited by chemogenetic H2O2 synthesis, Redox Biol. 36 (2020) 101605, https://doi.org/10.1016/j.redox.2020.101605.

[10] A. Ghaffari Zaki, Y.C. Erdoğan, T. Akgul Caglar, E. Eroglu, Chemogenetic approaches to dissect the role of H2O2 in redox-dependent pathways using genetically encoded biosensors, Biochem. Soc. Trans. 50 (2022) 335–345, https://doi.org/10.1042/BST20210506.

[11] A. Sorrentino, B. Steinhorn, L. Troncone, S.S.S. Saravi, S. Badole, E. Eroglu, M. F. Kijewski, S. Divakaran, M. Di Carli, T. Michel, Reversal of heart failure in a chemogenetic model of persistent cardiac redox stress, Am. J. Physiol. Heart Circ. Physiol. 317 (2019) H617–H626, https://doi.org/10.1152/ajpheart.00177.2019.

[12] E. Eroglu, B. Gottschalk, S. Charoensin, S. Blass, H. Bischof, R. Rost, C.T. Madreiter-Sokolowski, B. Pelzmann, E. Bernhart, W. Sattler, S. Hallström, T. Malinski, M. Waldeck-Weiermair, W.F. Graier, R. Malli, Development of novel FP-based probes for live-cell imaging of nitric oxide dynamics, Nat. Commun. 7 (2016) 10623, https://doi.org/10.1038/ncomms10623.

[13] E. Eroglu, R. Rost, H. Bischof, S. Blass, A. Schreilechner, B. Gottschalk, M. R. Depaoli, C. Klec, S. Charoensin, C.T. Madreiter-Sokolowski, J. Ramadani, M. Waldeck-Weiermair, W.F. Graier, R. Malli, Application of genetically encoded fluorescent nitric oxide (NO•) probes, the geNOps, for real-time imaging of NO• signals in single cells, JoVE (2017) 55486, https://doi.org/10.3791/55486.

[14] M. Opelt, E. Eroglu, M. Waldeck-Weiermair, M. Russwurm, D. Koesling, R. Malli, W.F. Graier, J.T. Fassett, A. Schrammel, B. Mayer, Formation of nitric oxide by aldehyde dehydrogenase-2 is necessary and sufficient for vascular bioactivation of nitroglycerin, J. Biol. Chem. 291 (2016) 24076–24084, https://doi.org/10.1074/jbc.M116.752071.

[15] E. Eroglu, H. Bischof, S. Charoensin, M. Waldeck-Weiermaier, W.F. Graier, R. Malli, Real-time imaging of nitric oxide signals in individual cells using geNOps, in: A. Mengel, C. Lindermayr (Eds.), Nitric Oxide: Methods and Protocols, Springer, New York, NY, 2018, pp. 23–34, https://doi.org/10.1007/978-1-4939-7695-9_3.

[16] E. Eroglu, S. Hallström, H. Bischof, M. Opelt, K. Schmidt, B. Mayer, M. Waldeck-Weiermair, W.F. Graier, R. Malli, Real-time visualization of distinct nitric oxide generation of nitric oxide synthase isoforms in single cells, Nitric Oxide 70 (2017) 59–67, https://doi.org/10.1016/j.niox.2017.09.001.

[17] S. Charoensin, E. Eroglu, M. Opelt, H. Bischof, C.T. Madreiter-Sokolowski, A. Kirsch, M.R. Depaoli, S. Frank, A. Schrammel, B. Mayer, M. Waldeck-Weiermair, W.F. Graier, R. Malli, Intact mitochondrial Ca2+ uniport is essential for agonist-induced activation of endothelial nitric oxide synthase (eNOS), Free Radic. Biol. Med. 102 (2017) 248–259, https://doi.org/10.1016/j.freeradbiomed.2016.11.049.

[18] M. Opelt, G. Wölkart, E. Eroglu, M. Waldeck-Weiermair, R. Malli, W.F. Graier, A. Kollau, J.T. Fassett, A. Schrammel, B. Mayer, A.C.F. Gorren, Sustained Formation of nitroglycerin-derived nitric oxide by aldehyde dehydrogenase-2 in vascular smooth muscle without added reductants: implications for the development of nitrate tolerance, Mol. Pharmacol. 93 (2018) 335–343, https://doi.org/10.1124/mol.117.110783.

[19] E. Eroglu, S. Hallström, H. Bischof, M. Opelt, K. Schmidt, B. Mayer, M. Waldeck-Weiermair, W.F. Graier, R. Malli, Real-time visualization of distinct nitric oxide generation of nitric oxide synthase isoforms in single cells, Nitric Oxide 70 (2017) 59–67, https://doi.org/10.1016/j.niox.2017.09.001.

[20] E. Eroglu, S.S.S. Saravi, A. Sorrentino, B. Steinhorn, T. Michel, Discordance between eNOS phosphorylation and activation revealed by multispectral imaging and chemogenetic methods, Proc. Natl. Acad. Sci. USA 116 (2019) 20210–20217, https://doi.org/10.1073/pnas.1910942116.

[21] G. Sevimli, M.J. Smith, T.A. Caglar, Ş. Bilir, M. Secilmis, H.Y. Altun, E.N. Yigit, F. Yang, T.P. Keeley, R. Malli, G. Öztürk, G.E. Mann, E. Eroglu, Nitric oxide biosensor uncovers diminished ferrous iron-dependency of cultured cells adapted to physiological oxygen levels, Redox Biol. 53 (2022) 102319, https://doi.org/10.1016/j.redox.2022.102319.

[22] T.P. Keeley, G.E. Mann, Defining physiological normoxia for improved translation of cell physiology to animal models and humans, Physiol. Rev. 99 (2019) 161–234, https://doi.org/10.1152/physrev.00041.2017.

[23] T. Keeley, R. Siow, R. Jacob, G. Mann, A PP2A-mediated feedback mechanism controls Ca 2+ -dependent NO synthesis under physiological oxygen, Faseb. J. 31 (2017), https://doi.org/10.1096/fj.201700211R fj.201700211R.

[24] T.P. Keeley, R.C.M. Siow, R. Jacob, G.E. Mann, Reduced SERCA activity underlies dysregulation of Ca2+ homeostasis under atmospheric O2 levels, Faseb. J. 32 (2018) 2531–2538, https://doi.org/10.1096/fj.201700685RRR.

[25] G. Warpsinski, M.J. Smith, S. Srivastava, T.P. Keeley, R.C.M. Siow, P.A. Fraser, G. E. Mann, Nrf2-regulated redox signaling in brain endothelial cells adapted to physiological oxygen levels: consequences for sulforaphane mediated protection against hypoxia-reoxygenation, Redox Biol. 37 (2020) 101708, https://doi.org/10.1016/j.redox.2020.101708.

[26] S.J. Chapple, T.P. Keeley, D. Mastronicola, M. Arno, G. Vizcay-Barrena, R. Fleck, R. C.M. Siow, G.E. Mann, Bach1 differentially regulates distinct Nrf2-dependent genes in human venous and coronary artery endothelial cells adapted to physiological oxygen levels, Free Radic. Biol. Med. 92 (2016) 152–162, https://doi.org/10.1016/j.freeradbiomed.2015.12.013.

[27] M. Secilmis, H.Y. Altun, J. Pilic, Y.C. Erdogan, Z. Cokluk, B.N. Ata, G. Sevimli, A. G. Zaki, E.N. Yigit, G. Öztürk, R. Malli, E. Eroglu, A Co-Culture-Based multiparametric imaging technique to dissect local H2O2 signals with targeted HyPer7, Biosensors 11 (2021) 338, https://doi.org/10.3390/bios11090338.

[28] F. Yang, M.J. Smith, A. Griffiths, A. Morrell, S.J. Chapple, R.C.M. Siow, T. Stewart, W. Maret, G.E. Mann, Vascular protection afforded by zinc supplementation in human coronary artery smooth muscle cells mediated by NRF2 signaling under hypoxia/reoxygenation, Redox Biol. 64 (2023) 102777, https://doi.org/10.1016/j.redox.2023.102777.

[29] H. Hwangbo, S.Y. Kim, H. Lee, S.-H. Park, S.H. Hong, C. Park, G.-Y. Kim, S.-H. Leem, J.W. Hyun, J. Cheong, Y.H. Choi, Auranofin enhances sulforaphane-mediated apoptosis in hepatocellular carcinoma Hep3B cells through inactivation of the PI3K/Akt signaling pathway, Biomol Ther (Seoul) 28 (2020) 443–455, https://doi.org/10.4062/biomolther.2020.122.

[30] H. Sies, V.V. Belousov, N.S. Chandel, M.J. Davies, D.P. Jones, G.E. Mann, M. P. Murphy, M. Yamamoto, C. Winterbourn, Defining roles of specific reactive oxygen species (ROS) in cell biology and physiology, Nat. Rev. Mol. Cell Biol. 23 (2022) 499–515, https://doi.org/10.1038/s41580-022-00456-z.

[31] C.J. Edgell, C.C. McDonald, J.B. Graham, Permanent cell line expressing human factor VIII-related antigen established by hybridization, Proc. Natl. Acad. Sci. U. S. A. 80 (1983) 3734–3737, https://doi.org/10.1073/pnas.80.12.3734.

[32] E. Eroğlu, Simultaneous manipulation and imaging of chemogenetically induced hydrogen peroxide in hardly transfectable endothelial cells, CSJ 43 (2022) 645–651, https://doi.org/10.17776/csj.1114125.

[33] H.S. Kim, G.-H. Hwang, H.K. Lee, T. Bae, S.-H. Park, Y.J. Kim, S. Lee, J.-H. Park, S. Bae, J.K. Hur, CReVIS-Seq: a highly accurate and multiplexable method for genome-wide mapping of lentiviral integration sites, Molecular Therapy - Methods & Clinical Development 20 (2021) 792–800, https://doi.org/10.1016/j.omtm.2020.10.012.

[34] S. Hacein-Bey-Abina, C. Von Kalle, M. Schmidt, M.P. McCormack, N. Wulffraat, P. Leboulch, A. Lim, C.S. Osborne, R. Pawliuk, E. Morillon, R. Sorensen, A. Forster, P. Fraser, J.I. Cohen, G. de Saint Basile, I. Alexander, U. Wintergerst, T. Frebourg, A. Aurias, D. Stoppa-Lyonnet, S. Romana, I. Radford-Weiss, F. Gross, F. Valensi, E. Delabesse, E. Macintyre, F. Sigaux, J. Soulier, L.E. Leiva, M. Wissler, C. Prinz, T. H. Rabbitts, F. Le Deist, A. Fischer, M. Cavazzana-Calvo, LMO2-associated clonal T cell proliferation in two patients after gene therapy for SCID-X1, Science 302 (2003) 415–419, https://doi.org/10.1126/science.1088547.

[35] M. Bokhoven, S.L. Stephen, S. Knight, E.F. Gevers, I.C. Robinson, Y. Takeuchi, M. K. Collins, Insertional gene activation by lentiviral and gammaretroviral vectors, J. Virol. 83 (2009) 283–294, https://doi.org/10.1128/JVI.01865-08.

[36] E. Ustyantseva, S.V. Pavlova, A.A. Malakhova, K. Ustyantsev, S.M. Zakian, S. P. Medvedev, Oxidative stress monitoring in iPSC-derived motor neurons using genetically encoded biosensors of H2O2, Sci. Rep. 12 (2022) 8928, https://doi.org/10.1038/s41598-022-12807-z.

[37] M.J. Smith, F. Yang, A. Griffiths, A. Morrell, S.J. Chapple, R.C.M. Siow, T. Stewart, W. Maret, G.E. Mann, Redox and metal profiles in human coronary endothelial and smooth muscle cells under hyperoxia, physiological normoxia and hypoxia: effects of NRF2 signaling on intracellular zinc, Redox Biol. 62 (2023) 102712, https://doi.org/10.1016/j.redox.2023.102712.

[38] R. Rodriguez-Rodriguez, E. Stankevicius, M.D. Herrera, L. Østergaard, M. R. Andersen, V. Ruiz-Gutierrez, U. Simonsen, Oleanolic acid induces relaxation and calcium-independent release of endothelium-derived nitric oxide, Br. J. Pharmacol. 155 (2008) 535–546, https://doi.org/10.1038/bjp.2008.289.